

Research Article

Graphene Supported Pt–Ru–Sn Electrocatalyst for Borohydride Oxidation in Membraneless Borohydride Fuel Cell

M. Elumalai¹, M. Priya¹, S. Kiruthika², B. Muthukumar^{1,*}

¹Department of Chemistry, Presidency College, Chennai – 600 005, India.

²Department of Chemical Engineering, SRM University, Chennai – 603 203, India.

*Corresponding author's e-mail: dr.muthukumar@yahoo.com

Abstract

Graphene supported Pt–Ru–Sn trimetallic electrocatalysts are prepared by a modified sodium borohydride reduction method in aqueous solution at room temperature, and used as the anode electrocatalysts for membraneless borohydride fuel cell. The physical and electrochemical properties of the as-prepared electrocatalysts are investigated by X-ray diffraction (XRD) analysis, transmission electron microscopy (TEM), cyclic voltammetry (CV), chronoamperometry (CA) and fuel cell test. XRD results show that the diffraction peaks in Pt–Ru–Sn/G catalysts shift slightly to lower 2θ values compared with that of Pt/G catalyst, suggesting the formation of Pt–Ru–Sn alloying. TEM results show that the morphologies of Pt–Ru–Sn trimetallic catalysts are uniformly spherical with the particle size of about 3.5 nm on the graphene surface. Besides, it has been found that the Pt–Ru–Sn catalysts have much higher catalytic activity for the oxidation of sodium borohydride than Pt/G catalyst, especially the Pt–Ru–Sn/G (60:30:10) catalyst presents the highest catalytic activity among all as-prepared catalysts. The membraneless borohydride fuel cell with Pt–Ru–Sn/G (60:30:10) anode catalyst and Pt/G cathode catalyst obtains the maximum power density as high as 39.61 mW cm^{-2} at room temperature.

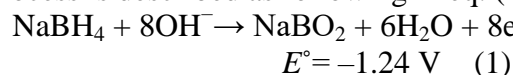
Keywords: Graphene; Electrocatalysts; Platinum; Ruthenium; Tin; Membraneless Borohydride Fuel Cell.

Introduction

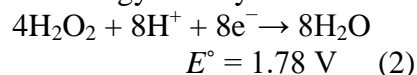
Fuel cells which are capable of consuming liquid fuels directly have attracted worldwide attention for their portability and mobile applications, as they are convenient, safe and easy fuel storage systems [1]. Among the various types of fuel cells, membraneless fuel cell is considered as a promising candidate for miniature appliances [1-4]. Membraneless fuel cell is a device that incorporated into single micro structured manifold using all the fundamental components of the fuel cells. Membraneless fuel cells also called laminar flow-based fuel cells eliminate the use of proton exchange membrane as they utilize the co-laminar flow nature of multistream in a single microfluidic channel to separate the anolyte and the catholyte [5-7]. Membraneless borohydride fuel cells (MLBFCs) overwhelmed many problems associated with polymer electrolyte membrane-based fuel cells such as membrane degradation, humidification, fuel crossover, and water management. [2]. The BH_4^- -based fuel cell

utilizes chemically stored energy in the BH_4^- anion which is provided in the form of sodium borohydride (NaBH_4). NaBH_4 is of high-energy density (9.3 Wh.g^{-1}), thus rendering it a promising energy as well as hydrogen storage compound [3-4]. The absence of C–C bond cleavage simplifies its fuel oxidation considerably.

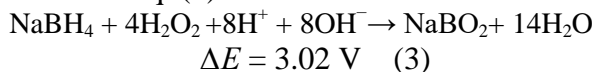
Additionally, the use of alkaline electrolytes, which feature relatively low corrosion activity, opens up the possibility of applying readily available, low-cost, nonprecious, metal anode catalysts. The anode reaction in an aqueous alkaline medium according to an eight-electron process is described as following in eq. (1) [5]:



With the oxidation of NaBH_4 at the anode, the hydrogen peroxide in an acid electrolyte instead of oxygen as an oxidant can yield higher cell potential and energy density:



In combination with the reduction of hydrogen peroxide, MLBFC can give a theoretical cell voltage of 3.02 V and present a high energy density. Over all cell reaction is as follow in eq. (3):



Supporting material considerably affects the catalytic characteristics of Pt-based electrocatalysts. Predominantly, carbon materials have been examined for their use as catalyst supports for fuel cells, such as Vulcan XC-72R carbon [6], carbon nanotubes (CNTs) [7], carbon nanofibers [8], graphene [9] and mesoporous carbon [10,11]. Among them, graphene possesses some unique properties which make it one of the most interesting materials nowadays, and occupies a similar level in new applications such as CNTs. Some exclusive properties of graphene are as follows: it has a high theoretical surface area of about 2,620 m²/g [12-14]; it is chemically stable and almost impermeable to gases; it can withstand large electrical densities; it has high thermal [15] and chemical conductivity [16]; it possesses outstanding mechanical properties; and boasts of its relatively low cost of production compared to CNTs [17]. These properties make graphene a promising catalyst carrier in the next generation of carbon-based supports for electrocatalysts.

Many studies have been carried out indicating that Pt is one of the most attractive metal catalysts for the anode catalysts of BH₄-based fuel cells [18]. However, Pt is a noble metal, the usage of which in fuel cell application has to be cut down before this technology can be commercialized. It is well known that addition of metals to a Pt catalyst is an effective way to reduce the cost of the catalyst. Furthermore, bimetallic catalysts could achieve higher catalytic activity and stability than monometallic ones. Tarozaita *et al.* [19] prepared three such from Pt–Sn complexes of H₃[Pt(SnCl₃)₃], H₂[Pt(SnCl₃)₂Cl₂], and H₂[Pt₃(SnCl₃)₈], and the BH₄[−] electrooxidation on the glassy carbon electrode modified by the three complex solutions were studied. However, Pt–Sn/G and Pt–Ru/G catalysts have received more attention in the performance of fuel cells [20]. Comparing the electrocatalytic activity of Pt–Sn/G and Pt–Ru/G catalysts, Pt–Sn/G electrocatalyst has been more active than the Pt–Ru/G electrocatalyst for NaBH₄ oxidation at room temperature [21].

Nevertheless, efforts are being made to improve the performance of Pt–Ru/G anode catalysts for oxidation of NaBH₄ to a suitable level for the purpose of commercialization. To promote the catalytic activity of Pt–Ru/G electrocatalysts, Sn was added as a third metal. Graphene-supported Pt–Ru–Sn trimetallic electrocatalyst has higher catalytic activity than other catalysts, this is due to their electronic effect (Fig.1).

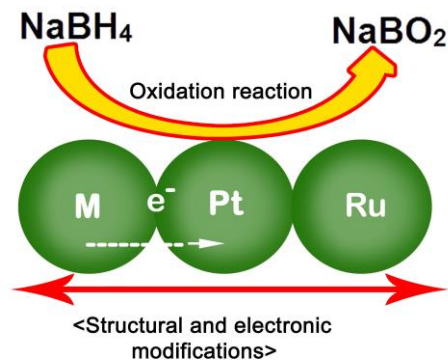


Fig. 1. A schematic diagram of Structural and electronic effect of Pt–Ru–M (M= Sn) ternary catalysts

In the present work, a series of Pt–Ru–Sn/G catalyst were synthesized by modified NaBH₄ reduction method in aqueous solution at room temperature, and used as the anode catalyst for sodium borohydride electro-oxidation. The prepared electrocatalysts are characterized using transmission electron microscope (TEM), energy dispersive X-ray (EDX) analysis and X-ray diffraction (XRD) analysis. Sodium borohydride in the presence of above catalysts was studied using cyclic voltammetry (CV) and chronoamperometry (CA). Lastly, the catalysts were tested as the anode in membraneless borohydride fuel cell.

Materials and methods

Materials and reagents

The metal precursors used for the preparation of electrocatalysts were H₂PtCl₆ (from Aldrich), RuCl₃·3H₂O (from Alfa Aesar), and SnCl₂·2H₂O (from Sigma Aldrich). Graphene (purity of 97%, from Graphene Supermarket Supply) was used as a support for the catalysts. Graphite Plates (3 cm long and 0.1 cm wide, from E-TEK) were used as substrates for the catalyst to prepare the electrodes. Nafion[®] (DE 521, Dupont USA) dispersion was used to make the catalyst slurry. Isopropyl alcohol (from Merck) was used as a solvent.

Sodium Borohydride (from Merck) was used as the fuel and reducing agent and sodium perborate (from Riedel) was used as an oxidant. Sodium hydroxide (from Merck), and H₂SO₄ (from Merck) were used as electrolyte for fuel and oxidant respectively. All the chemicals were of analytical grade. Pt/G (40-wt%, from E-TEK) was used as the cathode catalyst.

Catalyst preparation

Graphene supported ternary Pt–Ru–Sn catalysts with different atomic ratios were synthesized by using a conventional reduction method with NaBH₄ [22]. The graphene was ultrasonically dispersed in a mixture of ultrapure water (Millipore MilliQ, 18 MΩ cm), and isopropyl alcohol for 20 min. The precursors were added to the ink and then mixed thoroughly for 15 min. The pH value of the ink was adjusted by NaOH solution to 8 and then raised its temperature to 80 °C. Twenty-five milliliters of 0.2 mol L⁻¹ solution of sodium hydroxide was added into the ink drop by drop, and the bath was stirred for 1 h. The mixture was cooled, dried and washed repeatedly with deionized (DI) water until no Cl⁻ ions existed. The catalyst powder was dried for 3 h at 120°C and stored in a vacuum vessel. For comparison, the monometallic Pt/G, bimetallic Pt–Ru/G and Pt–Sn/G catalysts were synthesized under the same conditions. The electrocatalytic mixtures and atomic ratios were Pt/G (100), Pt–Ru/G (50:50), Pt–Sn/G (50:50), Pt–Ru–Sn/G (60:10:30), Pt–Ru–Sn/G (60:20:20) and Pt–Ru–Sn/G (60:30:10). The nominal loading of metals in the electrocatalysts was 40 %wt and rest 60 %wt was graphene.

Physical characterization

TEM (Philips CM 12 Transmission Electron Microscope) were used to evaluate the particle size distribution and mean particle size. The crystal structure of the synthesized electrocatalysts was characterized by powder X-ray diffraction (XRD) using a Rigaku multiflex diffractometer (model RU-200 B) with Cu–K_{α1} radiation source ($\lambda_{K\alpha 1} = 1.5406 \text{ \AA}$) operating at room temperature. The tube current was 40 mA with a tube voltage of 40 kV. The 2θ angular regions between 20° and 90° were recorded at a scan rate 5° min⁻¹ the mean particle size analyzed from TEM is verified by determining the crystallite size from XRD pattern using

“Scherer” formula. Pt (2 2 0) diffraction peak was selected to calculate crystallite size and lattice parameter of platinum. According to Scherrer’s eq. (4) [23].

$$d = \frac{0.9\lambda_{K\alpha 1}}{\beta_{2\theta} \cos \theta_{\max}} \quad (4)$$

Where D is the average crystallite size, θ_{\max} is the angle at the position of the peak maximum, $\beta_{2\theta}$ is the half width of the peak (in radians), 0.9 is the shape factor for spherical crystallite and $\lambda_{K\alpha 1}$ is the wavelength of X-rays used. The lattice parameters of the catalysts were estimated according to equation (5) [24].

$$a = \frac{\sqrt{2} \lambda_{K\alpha 1}}{\sin \theta_{\max}} \quad (5)$$

Where a is the lattice parameter (nm) and all the other symbols have the same meanings as in equation 5. The atomic ratio of the catalysts was determined by an energy dispersive X-ray (EDX) analyzer, which was integrated with the TEM instrument.

Electrochemical measurement

Electrochemical Measurements were performed using electrochemical workstation (CH Instruments, Model CHI6650, USA) interfaced with a personal computer using the CHI software, at room temperature. A conventional three-electrode electrochemical cell using cyclic voltammetry (CV) and Chronoamperometry (CA) techniques was used for measurements. Pt/G, Pt–Ru/G, Pt–Sn/G and different Pt–Ru–Sn/G catalysts coated with glassy carbon electrode (GCE, 3 mm diameter and 0.071 cm² of electrode area, from CHI, USA) were employed as a working electrode, a Pt sheet was used as a counter electrode and an Ag/AgCl in saturated KCl electrode was used as reference. The working electrode was prepared by applying catalyst ink made of 20 mg of electrocatalyst in a solution of 50 mL of water containing three drops of 6% PTFE suspension. The resulting mixture was treated in an ultrasound bath for 10 min to obtain a uniform dispersion. The catalyst slurry was then drop-cast on to a glassy carbon electrode and allowed to dry at 100°C for 30 min. for assessing the electrocatalytic activity of the working electrode; cyclic voltammetry was obtained in 0.15 M sodium borohydride and 3 M NaOH solution with a scan rate of 20 mV S⁻¹. For the durability

test, the chronoamperometric experiments were carried out at a potential step of -1.2 to -0.2 V for 600 s in the same electrolyte. Before each measurement, the solution was purged with high-purity nitrogen gas for at least 30 min to ensure oxygen-free measurements.

Single cell test

In the present work, we designed the membraneless borohydride fuel cell (MLBFC) by using a laminar flow-based fuel cell configuration [25–27]. In this MLBFC, sodium borohydride and sodium hydroxide solution used as a fuel, sodium perborate and sulfuric acid solution used as an oxidant, respectively. Sodium borohydride considered as one of the most promising combustible materials used in microfluidic fuel cells, because of its high-energy density, low toxicity, easy storage and transportation. Sodium perborate ($\text{NaBO}_3 \cdot 4\text{H}_2\text{O}$) is a nontoxic, cheap, environment friendly and large-scale industrial chemical, primarily used as a source of ‘active oxygen’ in detergents and as a mild antiseptic. In the crystalline state, sodium perborate existed as a dimeric peroxy-salt with water of hydration, but in the aqueous solution, it involved hydrogen peroxide [28, 29] as shown in eq. (6);



The byproduct is harmless and this stable and easily handled crystalline substance is used as oxidant in MLBFC.

In MLBFC, the aqueous fuel and oxidant streams flow in parallel in a single microchannel with the anode and cathode on opposing sidewalls (Fig.2). Graphite plates of one mm thickness served as current collectors and catalyst support structures. The different anode and cathode catalysts were coated onto the graphite plates. For single cell, the anode catalysts with different atomic ratios were prepared as follows: Pt/G (100). Pt–Ru/G (50:50), Pt–Sn/G (50:50), Pt–Ru–Sn/G (60:10:30), Pt–Ru–Sn/G (60:20:20) and Pt–Ru–Sn/G (60:30:10) with catalyst loading 2 mg/cm^2 was used in all experiments. The two catalyst-coated graphite plates were aligned to form a channel with 0.1 cm electrode-to-electrode distance (width), a 3 cm length, and a 0.1 cm height. The anolyte (fuel and electrolyte) and catholyte (oxidant and electrolyte) streams flow in a laminar fashion over the anode and cathode respectively. The electrode area along a

microchannel wall between the inlets and outlet (3 cm long and 0.1 cm wide) was used as the geometric surface area of the electrodes in this study (0.3 cm^2). The design is described in detail elsewhere [30, 31]. The anolyte used in the anode side was 0.15 M sodium borohydride + 3 M sodium hydroxide and catholyte used in the cathode side was 0.15 M sodium perborate + 1.5 M sulfuric acid. The flow rate of each of the streams was 0.3 mL min^{-1} (total flow rate of 0.6 mL min^{-1}). The MLBFC was operated at room temperature. The current-voltage characteristics of MLBFC were measured using an electrochemical workstation (CH Instruments, model CHI6650, USA) and the data was verified using a multi-meter (MASTECH[®] MAS8301).

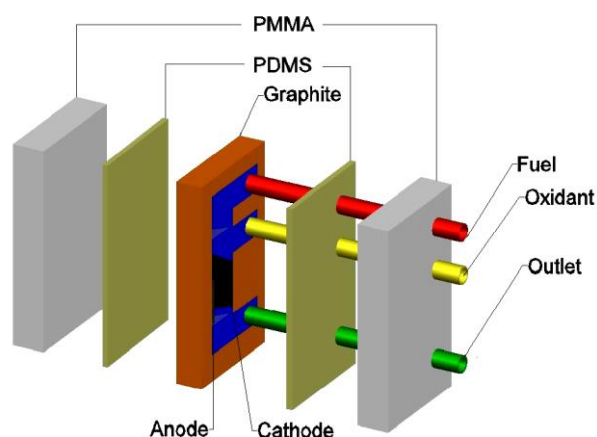


Fig. 2. Schematic of the E-shaped membraneless laminar flow based fuel cell with graphite plates molded with poly(dimethylsiloxane) (PDMS) and sealed with poly(methylmethacrylate) (PMMA)

Results and discussions

Physical characterization

X-ray Diffraction (XRD)

The XRD patterns of the prepared Pt–Ru–Sn/G (60:30:10), Pt–Ru–Sn/G (60:20:20), Pt–Ru–Sn/G (60:10:30), Pt–Ru/G (50:50), Pt–Sn/G (50:50) and Pt/G (100) catalysts are shown in Fig. 3. The first wide diffraction peak positioned at $2\theta = 25.0^\circ$ is attributed to the graphene (0 0 2) crystal face. The diffraction peak positioned at $2\theta = 39.70^\circ$, 46.70° , 67.50° and 81.30° could be indexed to the (1 1 1), (2 0 0), (2 2 0) and (3 1 1) planes of the face-centered cubic (fcc) Pt, which match well with the standard Pt peaks. The XRD of the pure Pt displays sharp and well-defined intense peaks, which indicates good crystallinity. The diffraction peaks of Pt–Ru/G (50:50) were

shifted towards higher 2θ values relative to those of Pt/G (100), whereas the peaks of Pt–Sn/G (50:50) were shifted towards lower angles which reveal the formation of a solid solution due to the incorporation of Sn into the fcc structure of Pt. It should be noted that the ternary Pt–Ru–Sn/G (60:30:10), Pt–Ru–Sn/G (60:20:20), Pt–Ru–Sn/G (60:10:30) catalyst shows intermediate 2θ values as compared to those of Pt–Ru/G (50:50), Pt–Sn/G (50:50) catalyst. Hence, the 2θ angle shift of the crystalline Pt peaks reveals the formation of an alloy caused by the incorporation of Ru and Sn into the Pt structure. On the other hand, the amount of Ru or Sn alloyed with Pt is usually less than nominally predicted, because some of these atoms were present as amorphous oxides. Therefore, no other diffraction peaks for metallic Ru, Sn or Ru, Sn oxide were detected in the Pt–Ru–Sn/G catalysts.

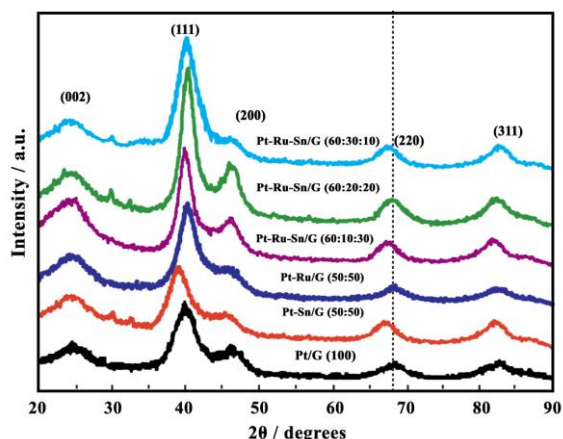


Fig. 3. X-ray diffraction patterns of Pt–Ru–Sn/G (60:30:10), Pt–Ru–Sn/G (60:20:20), Pt–Ru–Sn/G (60:10:30), Pt–Ru/G (50:50), Pt–Sn/G (50:50), and Pt/G (100) catalysts

The fcc lattice parameters were evaluated from the angular position of the (2 2 0) peaks. The lattice parameter of Pt/G catalyst ($a=$

0.3919) is smaller than that of the bulky metal ($a= 0.3923$ nm), and it has been ascribed to the interactions, or size effect, between Pt and carbon [33]. The lattice parameters of Pt–Ru/G (50:50), Pt–Sn/G (50:50), Pt–Ru–Sn/G (60:10:30), Pt–Ru–Sn/G (60:20:20) and Pt–Ru–Sn/G (60:30:10) electrocatalyst were 0.3883, 0.3983, 0.3933, 0.3927 and 0.3905 nm, respectively. Since the lattice parameter of the Pt–Ru–Sn/G was larger than that of the Pt–Ru/G and smaller than that of the Pt–Sn/G, the formation of a ternary Pt–Ru–Sn/G electrocatalyst was confirmed. The difference of lattice parameters and the shift of the (2 2 0) plane indicate interactions between Pt, Ru and Sn. The average particle sizes for Pt/G (100), Pt–Ru/G (50:50), Pt–Sn/G (50:50), Pt–Ru–Sn/G (60:10:30), Pt–Ru–Sn/G (60:20:20) and Pt–Ru–Sn/G (60:30:10) electrocatalysts were in the range of 3–5 nm, and were estimated using the scherrer equation (Table 1), which are in good agreement with the transmission electron microscope images. The crystallite size of ternary Pt–Ru–Sn/G catalysts is smaller than that of binary Pt–Ru/G and Pt–Sn/G catalysts prepared by same method.

Transmission Electron Microscopy (TEM)

Fig. 4 a-d shows TEM images and the corresponding particle size distribution histogram of graphene supported Pt, Pt–Ru, and Pt–Ru–Sn catalysts synthesized by conventional sodium borohydride reduction method. From the TEM image, the average particle diameter was found to be approximately 3-5 nm, which is in fairly good agreement with the data calculated from XRD. The particle size distribution of these catalysts is shown in Table 1 in accordance to TEM images.

Table 1. The EDX compositions, lattice parameters and the particle size obtained for different atomic ratios of electrocatalysts

Electrocatalysts	Nominal atomic ratio			EDX atomic ratio			lattice parameters (nm)	Crystallite size (nm)	Particle size from TEM (nm)
	Pt	Ru	Sn	Pt	Ru	Sn			
Pt/G	100	–	–	99	–	–	0.3919	5.0	4.7
Pt–Sn/G	50	–	50	51	–	49	0.3983	4.7	4.5
Pt–Ru/G	50	50	–	52	48	–	0.3883	4.5	4.3
Pt–Ru–Sn/G	60	10	30	62	09	29	0.3933	4.2	3.8
Pt–Ru–Sn/G	60	20	20	62	19	19	0.3927	4.1	3.7
Pt–Ru–Sn/G	60	30	10	62	29	09	0.3905	3.9	3.6

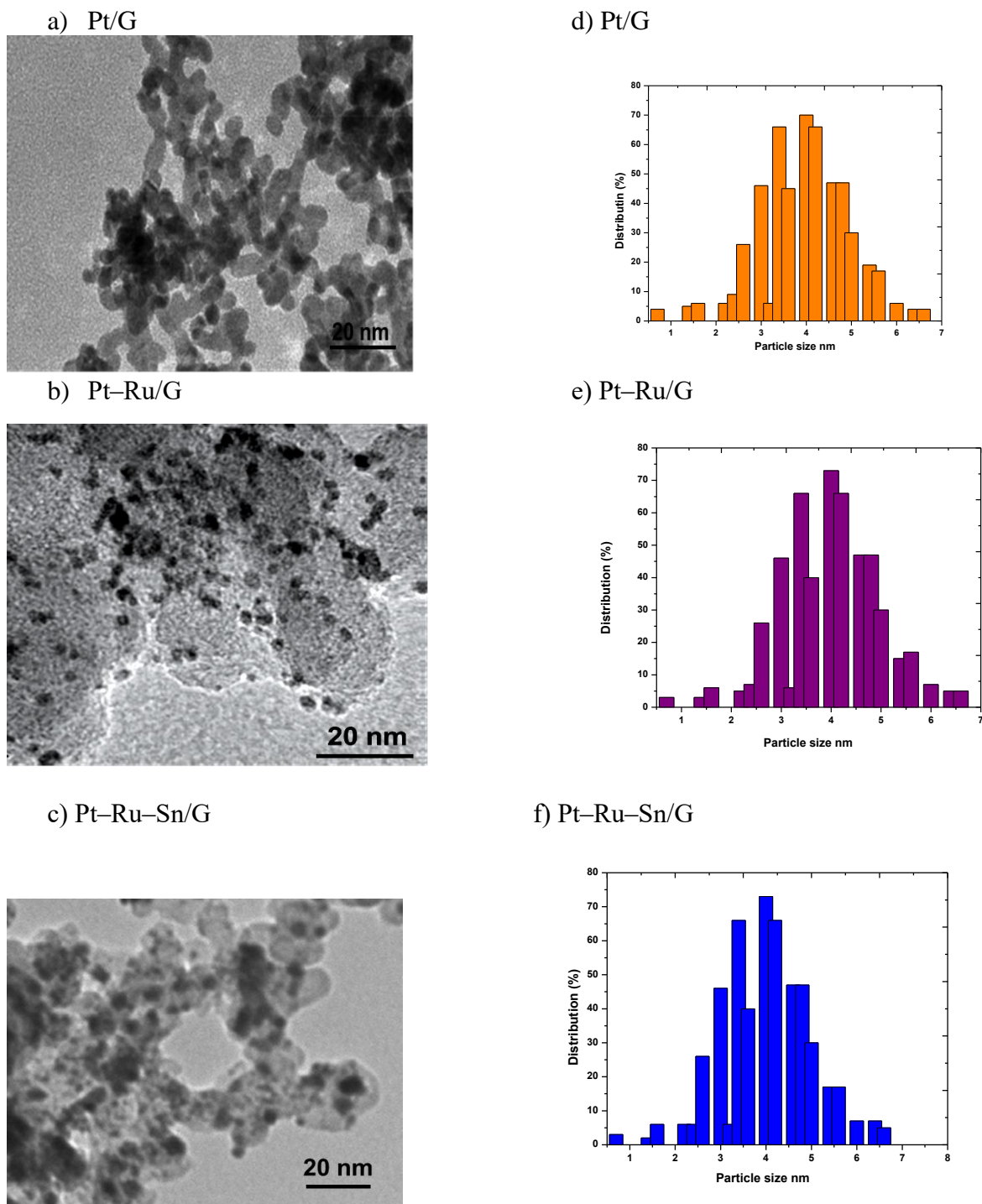


Fig. 4 (a-c) TEM image and (d-f) particle size distribution of Pt/G (100), Pt–Ru/G (50:50) and Pt–Ru–Sn/G (60:30:10) catalyst

Energy Dispersive X-ray Spectroscopy (EDX)

Energy dispersive X-ray spectroscopy is conducted by focusing the electron beam on several different selected regions of the graphene supported nanoparticles. EDX spectra of Pt/G, Pt–Sn/G, Pt–Ru/G and Pt–Ru–Sn/G nanoparticles are shown in Fig. 5 a-d. The average composition of the sample was in atomic ratio of Pt:Ru:Sn = 6:3:1. The EDX results of the ternary Pt–Ru–Sn/G catalysts are very close to

the nominal values, which indicate that the metals were loaded onto the graphene support without obvious loss.

Electrochemical characterization

Cyclic voltammetry

Fig. 6a shows the Cyclic Voltammogram (CV) on the Pt/G (100), Pt–Ru/G (50:50), Pt–Sn/G (50:50), Pt–Ru–Sn/G (60:20:20), Pt–Ru–Sn/G (60:10:30) and Pt–Ru–Sn/G (60:30:10) catalysts in 0.5 M sulphuric acid solution.

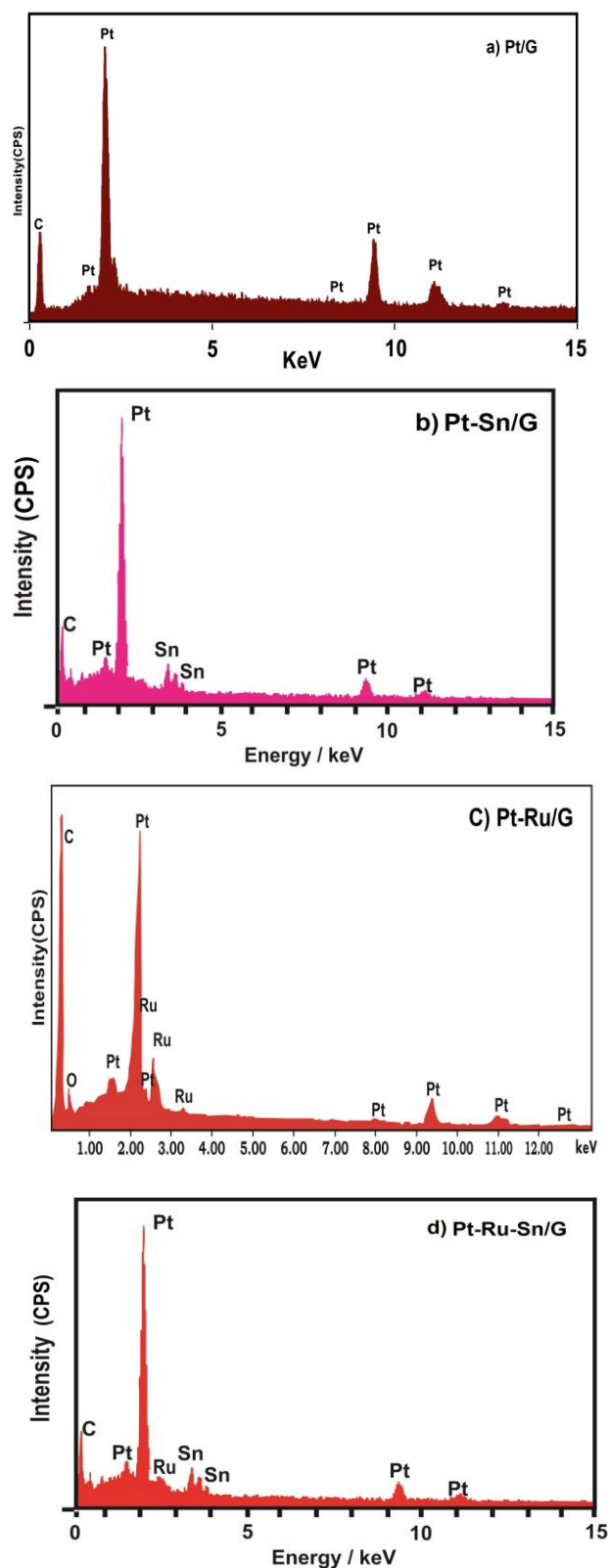


Fig. 5. EDX spectra of a) Pt/G, b) Pt–Sn/G c) Pt–Ru/G and d) Pt–Ru–Sn/G catalysts

The CV curves were obtained in a half cell at a scan rate of 50 mV s^{-1} between 0.05 and +1.2 V (Vs. Ag/AgCl) in the absence of sodium borohydride and it room temperature. The characteristic features of polycrystalline Pt, i.e. “hydrogen adsorption/desorption peak in high potential region”, oxide formation/stripping

wave/peaks in high potential region and a flat double layer in between, are observed for all the synthesized catalysts. The voltammograms of the electrocatalysts did not display a well-defined hydrogen region between 0.05 and 0.35 V, as the catalyst features in this region are influenced by their surface composition. The binary Pt–Ru/G (50:50), Pt–Sn/G (50:50) catalysts showed a voltammetric charge similar with reference to that of the pure Pt catalyst. However, a considerable increase in the voltammetric charge of ternary Pt–Ru–Sn/G (60:20:20), Pt–Ru–Sn/G (60:10:30) Pt–Ru–Sn/G (60:30:10) catalysts was observed in the double-layer region, indicating that the addition of Sn into binary Pt–Ru/G leads to an enhanced activity for the oxidation reactions. Thus, it can be concluded that the enhanced activity of Pt–Ru–Sn/G (60:30:10) for sodium borohydride electro-oxidation is mainly due to an intrinsic improvement in catalytic activity.

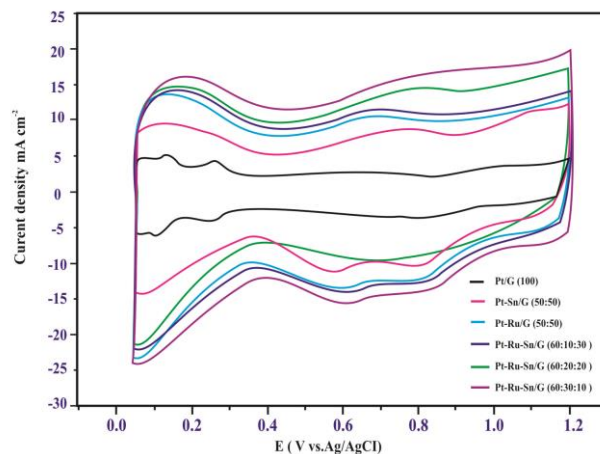


Fig. 6a. CVs of Pt–Ru–Sn/G (60:30:10), Pt–Ru–Sn/G (60:20:20), Pt–Ru–Sn/G (60:10:30), Pt–Ru/G (50:50), Pt–Sn/G (50:50), and Pt/G (100) catalysts in 0.5 M H_2SO_4

The cyclic voltammeteries (CV) recorded for Pt–Ru–Sn/G (60:30:10), Pt–Ru–Sn/G (60:20:20), Pt–Ru–Sn/G (60:10:30), Pt–Ru/G (50:50), Pt–Sn/G (50:50) and Pt/G (100) electrodes with 0.15 M NaBH_4 + 3 M NaOH solution at a scan rate of 20 mV s^{-1} in the potential range of -1.2 V to 0.6 V (vs. Ag/AgCl) are showed in Fig. 6b.

According to the CV curves, the electrochemical performance of BH_4^- is fairly complex and characterized by a number of oxidation peaks. During the forward sweep, at a scan rate of 20 mV s^{-1} , a well-defined oxidation peaks rises at about -0.81 V (a1), followed by a

broad hump anodic peak (a2) which is observed. During the reverse sweep, a sharp anodic spike (c1) is noticed. Analogous anodic-cathodic peak patterns in CV have been reported by Concha and Chatenet [1] and Gyenge [33].

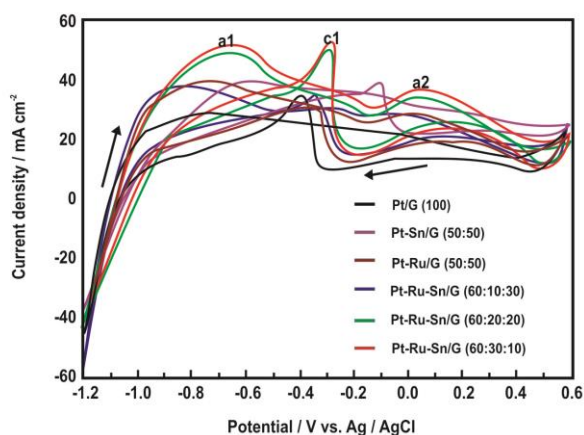


Fig. 6b. CVs of Pt–Ru–Sn/G (60:30:10), Pt–Ru–Sn/G (60:20:20), Pt–Ru–Sn/G (60:10:30), Pt–Ru/G (50:50), Pt–Sn/G (50:50), and Pt/G (100) catalysts in 0.15 M NaBH₄ + 3 M NaOH

The first anodic peak (a1) can be allocated to BH₄[−] hydrolysis followed by the electro-oxidation of H₂ (Eq. (7)), the second oxidation peak (a2) is attributed to the direct oxidation of BH[−] in the absence of H₂ electro-oxidation, and the peak (c1) is due to the oxidation of absorbed intermediate oxidation product of BH₃OH[−] (Eq. (8)) on the partially oxidized Pt surface.



The onset potential for the oxidation of NaBH₄ in a positive scan was a significant factor for evaluating the catalyst's activity. The onset

Table 2. CV results of Pt–Ru–Sn/G (60:30:10), Pt–Ru–Sn/G (60:20:20), Pt–Ru–Sn/G (60:10:30), Pt–Ru/G (50:50), Pt–Sn/G (50:50), and Pt/G (100) electrocatalysts at room temperature.

Catalyst	Scan rate 20 mV s ^{−1}	
	Positive peak potential (V vs. Ag/AgCl)	Peak current density (mA.cm ^{−2})
Pt/G (100)	0.0969	21.50
Pt–Sn/G (50:50)	0.0970	30.13
Pt–Ru/G (50:50)	0.0973	31.20
Pt–Ru–Sn/G (60:10:30)	0.1023	31.51
Pt–Ru–Sn/G (60:20:20)	0.0980	32.72
Pt–Ru–Sn/G (60:30:10)	0.0983	33.32

The CV results show that pure Pt/G (100) catalysts do not perform as an appropriate anode

potentials for the oxidation of NaBH₄ on the Pt–Ru–Sn/G (60:30:10) (−1.082 V), Pt–Ru–Sn/G (60:20:20) (−1.074 V) Pt–Ru–Sn/G (60:10:30) (−1.059 V) electrocatalysts is slightly lower than that on the Pt–Ru/G (50:50) (−1.050 V), Pt–Sn/G (50:50) (−1.035 V) catalysts. The CV curves illustrate the presence of a peak in the potential range of the positive sweep, and another peak in the negative sweep. The peak in the positive sweep is associated with the NaBH₄ oxidation, and the peak in the negative sweep is associated with the oxidation of BH₄ intermediate products from the partial oxidation of NaBH₄.

The peak current densities of peak a2 on Pt–Ru–Sn/G (60:30:10), Pt–Ru–Sn/G (60:20:20), Pt–Ru–Sn/G (60:10:30), Pt–Ru/G (50:50), Pt–Sn/G (50:50), and Pt/G (100) catalysts are 33.32, 32.72, 31.51, 31.20 30.13 and 21.50 mA cm^{−2}, respectively. Compared with Pt/G electrocatalyst, the peak current densities of peak a2 on Pt–Sn/G (50:50), Pt–Ru/G (50:50), Pt–Ru–Sn/G (60:10:30), Pt–Ru–Sn/G (60:20:20) and Pt–Ru–Sn/G (60:30:10) electrodes are increased 40.22%, 45.11%, 46.12%, 50.10% and 54.9%, respectively, indicating that the Pt–Ru–Sn/G (60:30:10) electrocatalysts can obviously improve the catalytic activity for BH₄[−] oxidation. Table 2 summarizes the cyclic voltammogram results of Pt–Ru–Sn/G (60:30:10), Pt–Ru–Sn/G (60:20:20), Pt–Ru–Sn/G (60:10:30), Pt–Ru/G (50:50), Pt–Sn/G (50:50) and Pt/G (100) electrocatalysts including the a2 peak of positive peak potential and the peak current densities of BOR.

for BOR, due to its hydrolysis of BH₄ that decreases the cell performance. However, the introduction of Ru and Sn promotes the

electrocatalysts' activity. CV for NaBH_4 oxidation reactions showed that the BH_4 hydrolysis was considerably inhibited by Pt–Ru–Sn/G (60:30:10), electrocatalyst, indicating the ability of Sn to promote direct oxidation of NaBH_4 .

Chronoamperometry

The Pt–Sn/G, Pt–Ru/G, and Pt–Ru–Sn/G electrocatalyst performances for borohydride oxidation were studied by chronoamperometry at a potential step of -1.2 to -0.2 V for 10 minutes, to evaluate the electrocatalytic activity of the catalysts. Fig. 7 shows representative chronoamperograms obtained for the different electrocatalysts whose current densities were normalized by Pt mass. During the first few minutes, there was a sharp decrease in the current density and after some time, it becomes relatively stable. It can be seen that the current density of sodium borohydride electro-oxidation on the Pt–Ru–Sn/G (60:30:10) catalyst is higher than that on the Pt–Ru–Sn/G (60:20:20), Pt–Ru–Sn/G (60:10:30), Pt–Ru/G (50:50), Pt–Sn/G (50:50), and Pt/G (100) catalyst at the same potentials. The activity change for sodium borohydride oxidation decreases in the order of Pt–Ru–Sn/G (60:30:10) > Pt–Ru–Sn/G (60:20:20) > Pt–Ru–Sn/G (60:10:30) > Pt–Ru/G (50:50) > Pt–Sn/G (50:50) > Pt/G (100), which is in fairly good agreement with our CV results for the durability test. Before each measurement, the solution was purged with high-purity nitrogen gas for at least 30 min to ensure oxygen-free measurements.

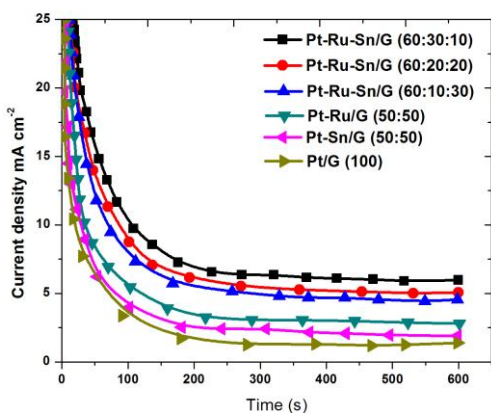


Fig. 7. Chronoamperometry of Pt–Ru–Sn/G (60:30:10), Pt–Ru–Sn/G (60:20:20), Pt–Ru–Sn/G (60:10:30), Pt–Ru/G (50:50), Pt–Sn/G (50:50), and Pt/G (100) electrocatalysts Single Cell Performance

Single fuel cell experiments were performed at room temperature on membraneless borohydride fuel cell using the Pt/G (100), Pt–Ru/G (50:50), Pt–Sn/G (50:50), Pt–Ru–Sn/G (60:10:30), Pt–Ru–Sn/G (60:20:20) and Pt–Ru–Sn/G (60:30:10) catalysts. The anolyte was 0.15 M NaBH_4 + 3M NaOH solution, and the catholyte was 0.15 M sodium perborate + 1.5 M H_2SO_4 solution. Fig. 8 shows the polarization curves and power density curves of the single MLBFCs obtained using Pt/G (100), Pt–Ru/G (50:50), Pt–Sn/G (50:50), Pt–Ru–Sn/G (60:10:30), Pt–Ru–Sn/G (60:20:20) and Pt–Ru–Sn/G (60:30:10) catalysts at room temperature. When Pt/G (100) was used as the anode catalyst, the performance of single cell was poor. The open circuit potential (OCP) was 1.65 V, probably caused by the mixed potential at the anode and cathode from the simultaneous oxidation of sodium borohydride and H_2 at the anode. The maximum output power density for Pt/G (100) is 7.75 mW cm^{-2} . The addition of Ru is considerably decreasing the sodium borohydride electro-oxidation reaction as observed from the polarization curves. The Ru content that provides maximum activity is in the range 30 at % of Ru: a decrease in the BOR activity for higher Ru contents is commonly ascribed to hindering access of the reactant to Pt sites by the presence of Ru oxide and/or low amounts of Pt sites; lower Ru contents depend on the degree of alloying. Above 30 at %, alloyed Ru hinders sodium borohydride adsorption by the ensemble effect. On these bases, the best compromise alloyed Ru in Pt–Ru/G catalysts should be 20–30 at %. Pt–Ru/G (50:50) (Ru 50 at %), Pt–Ru–Sn/G (60:10:30) (Ru 10 at.%), Pt–Ru–Sn/G (60:20:20) (Ru 20 at.%) and Pt–Ru–Sn/G (60:30:10) (Ru 30 at.%) showed OCP of 1.92 V, 2.23 V, 2.26 V and 2.29 V respectively. The comparison of both the bimetallic catalysts showed that peak power density of Pt–Ru/G (50:50) (16.99 mW cm^{-2}). The results of MLBFC adapting to different catalysts are summarized in Table 3.

When the current was normalized to the geometric area of single cell, it was observed that the cell performance of Pt–Ru–Sn/G (60:30:10) catalyst was better than other catalysts. In the low current discharging region, the power drawn from single cell was almost the same for all catalysts except Pt–Ru/G (50:50) and Pt/G (100).

Table 3. Summary of performance of fuel cell tests using 2 mg cm^{-2} catalyst loading, (40 wt% catalysts on graphene)

Anode Catalysts	Open circuit Potential (V)	Maximum power density (mW cm^{-2})	Maximum Current density (mA cm^{-2})
Pt/G (100)	1.65	7.75	25.639
Pt–Sn/G (50:50)	1.90	12.59	37.524
Pt–Ru/G (50:50)	1.92	16.79	45.695
Pt–Ru–Sn/G (60:10:30)	2.23	26.47	65.953
Pt–Ru–Sn/G (60:20:20)	2.26	35.53	77.201
Pt–Ru–Sn/G (60:30:10)	2.29	39.61	78.258

The cell voltage of Pt–Ru–Sn/G (60:30:10) at a current density of 51.21 mA cm^{-2} was 0.69 V which was higher than rest of the catalyst. In addition, there was a rapid initial fall in cell voltage for all catalysts, which was due to the slow initial sodium borohydride electro-oxidation reaction at the electrode surface. After an initial drop of 0.69 V the change in slope of the polarization curve for Pt–Ru–Sn/G (60:30:10) decreased, and it started drawing more current. This is attributed to the more effective catalytic ability of Pt–Ru–Sn/G

(60:30:10), once the sodium borohydride electro-oxidation reaction being initiated. Based on the power density drawn from single cell, Pt–Ru–Sn/G (60:30:10) is the best anode catalyst with peak power density value of 39.61 mW cm^{-2} . Moreover, as to Pt–Ru–Sn/G (60:30:10) catalyst, the replacement of 40% of Pt by Ru and Sn results in a large decrease of the catalyst cost. Thus Pt–Ru–Sn/G catalyst not only improves electrocatalytic activity of BH_4^- electro-oxidation for MLBFC, but also reduces the cost of the catalyst.

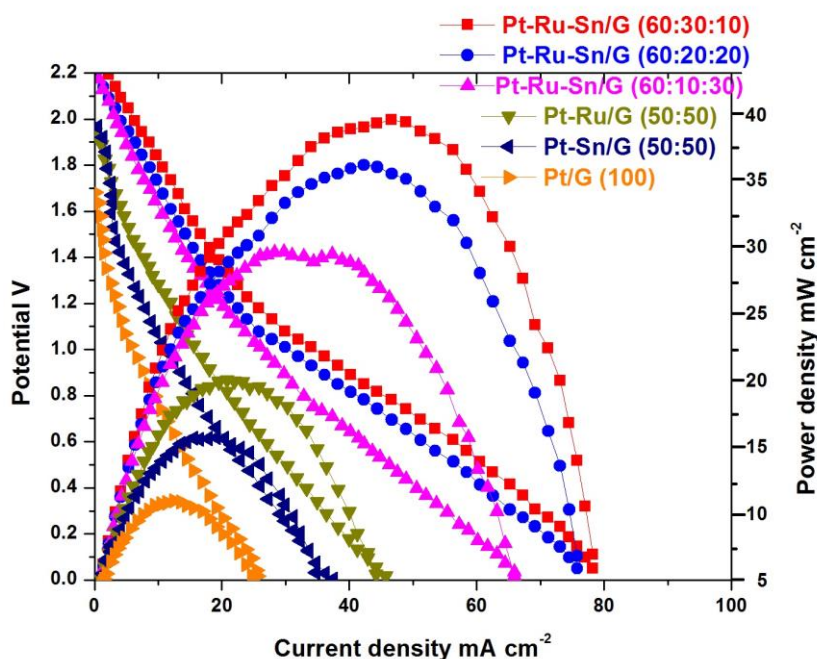


Fig. 8. Polarization and power density curves of different catalyst at 2 mg cm^{-2} catalyst loading on anode and cathode at room temperature. Anode feed: 0.15 M sodium borohydride in 3 M NaOH and Cathode feed: 0.15 M Sodium Perborate + 1.5 M H_2SO_4 . Stream flow rates: 0.3 ml min^{-1}

Conclusions

In the present study, Pt/G, Pt–Ru/G, Pt–Sn/G, and different Pt–Ru–Sn/G catalysts were synthesized according to the conventional sodium borohydride reduction method and examined as potential electrocatalysts for oxidation of borohydride ion. The catalytic

activity was assessed by cyclic voltammetry and chronoamperometry under conditions relevant for the anode catalysts layer composition of the membraneless borohydride fuel cell. The maximum activity for sodium borohydride oxidation was found for the Pt–Ru–Sn/G (60:30:10) than the Pt–Ru–Sn/G (60:20:20), Pt–

Ru–Sn/G (60:10:30), Pt–Ru/G (50:50), Pt–Sn/G (50:50) and Pt/G (100) catalysts. The significantly enhanced catalytic activity for sodium borohydride oxidation can be attributed to the high dispersion of ternary catalysts and to Sn acting as a promoting agent. XRD results show the homogeneous alloy structure of Pt, Ru and Sn. The TEM images indicated an average particle size of Pt–Ru–Sn/G (60:30:10) nanoparticle of 3–5 nm. The atom ratio of Pt, Ru and Sn from EDX analyses is close agreement with the original precursor concentration. The composition of ternary Pt–Ru–Sn/G (60:30:10) nanoparticles can be conveniently controlled by adjusting the initial metal salt solution and preparation conditions. Thus, the Pt–Ru–Sn/G (60:30:10) catalyst with both high electrocatalytic performance and low cost may serve as a promising anode catalyst for MLBFCs. We expect that the MLBFC may be a hopeful candidate for practical fuel cells to establish a clean and sustainable energy future.

Conflict of interest

Authors declare there are no conflicts of interest.

References

- [1] Concha BM, Chatenet M. Direct Oxidation of Sodium Borohydride on Pt, Ag and Alloyed Pt-Ag Electrodes in Basic Media. Part I: Bulk Electrodes. *Electrochim Acta*. (2009);54(26):6119–6129.
- [2] Concha BM, Chatenet M. Direct Oxidation of Sodium Borohydride on Pt, Ag and Alloyed Pt-Ag Electrodes in Basic Media: Part II. Carbon-Supported Nanoparticles. *Electrochim Acta*. 2009;54(26):6130–6139.
- [3] Grimmer C, Friedrich T, Woissetschlager D, Mayer N, Kalb R, Hacker V. Novel Borohydride-Based Ionic Liquids as Hydrogen Carrier. *Chemie Ing Tech*. 2014;86(9):1443–1443.
- [4] Grimmer C, Nestl S, Senn J, Hacker V. Selective Real-time Quantification of Hydrogen within Mixtures of Gases via an Electrochemical Method. *Int J Hydrogen Energy*. 2015;40(4):2055–2061.
- [5] Yang H, Coutanceau C, Leger JM, Alonso-Vante N, Lamy C. Methanol tolerant oxygen reduction on carbon-supported Pt–Ni alloy nanoparticles. *J Electroanal Chem*. 2005;576(2):305–313.
- [6] Lobato J, Ca nizares P, Rodrigo MA, Linares JJ, Lopez-Vizcaino R. Performance of a Vapor-Fed Polybenzimidazole (PBI)-Based Direct Methanol Fuel Cell. *Energy Fuels*. 2008;22(5):3335–3345.
- [7] Hsieh CT, Lin JY. Fabrication of bimetallic Pt–M (M= Fe, Co, and Ni) nanoparticle/carbon nanotubes electrocatalysts for direct methanol fuel cells. *J. Power Sources*. 2009;188(2):347–352.
- [8] Lobato CJ, Ca nizares P, Ubeda D, Pinar FJ, Rodrigo MA. Testing PtRu/CNF catalysts for a high temperature polybenzimidazole-based direct ethanol fuel cell. Effect of metal content. *Appl Catal B: Environ*. 2011;106(2):174–180.
- [9] Priya M, Elumalai M, Kiruthika S, Muthukumar B. Influences of supporting materials for Pt-Ru binary catalyst in Ethanol fuel cell, *International Journal of Modern Science and Technology*. 2016;1(1):5–11.
- [10] John S, Dutta I, Angelopoulos AP. Enhanced Electrocatalytic Oxygen Reduction through Electrostatic Assembly of Pt Nanoparticles onto Porous Carbon Supports from SnCl₂-Stabilized Suspensions. *Langmuir*. 2011;27(10):5781–5791.
- [11] Qi J, Jiang L, Wang S, Sun G. Synthesis of graphitic mesoporous carbons with high surface areas and their applications in direct methanol fuel cells. *Appl Catal B: Environ*. 2011;107(2):95–103.
- [12] Li Y, Tang L, Li J. Preparation and electrochemical performance of methanol oxidation of Pt/graphene Nanocomposites. *Electrochem Commun*. 2009;11(4):846–849.
- [13] Dong L, Gari RRS, Li Z, Craig MM, Hou S. Graphene-supported platinum and platinum-ruthenium nanoparticles with high electrocatalytic activity for methanol and ethanol oxidation. *Carbon*. 2010;48(3):781–787.
- [14] Lian P, Zhu X, Liang S, Li Z, Yang W, Wang H. Large reversible capacity of high quality graphene sheets as an anode material for lithium-ion batteries, *Electrochim Acta*. 2010;55(12):3909–3914.
- [15] Leenearts O, Partoens B, Peeters FM. Adsorption of small molecules on

- graphene, *J Microelectr.* 2009;40(5):860–862.
- [16] Mahendran S, Anbuselvan C. Kinetics and mechanism of oxidation of 5-(4'-bromophenyl)-5-oxopentanoic acid by acid permanganate. *International Journal of Modern Science and Technology.* 2016; 3(1):106–110.
- [17] Liu S, Wang J, Zeng J, Ou J, Li Z, Liu X, Yang S. Green electrochemical synthesis of Pt/Graphene sheet nanocomposite film and its electrocatalytic property. *J Power Sources.* 2010;195(15):4628–4633.
- [18] Kim JH, Kim HS, Kang YM, Song MS, Rajendran S, Han SC, Jung DH, Lee JY. Carbon-supported and unsupported Pt anodes for direct borohydride liquid fuel cells. *J Electrochem Soc.* 2004;151(7): A1039-A1043.
- [19] Zhenyuan J, Xiaoping S, Guoxing Z, Kangmin C, Guohua F, Lei T. Enhanced electrocatalytic performance of Pt-based nanoparticles on reduced graphene oxide for methanol oxidation. *J Electroanal Chem.* 2012;682:95–100.
- [20] Sungyool B, Byungchul J, Seunghee W and Yuanzhe P. Enhanced electrocatalytic activity of solvothermal graphene supported PtRu catalyst toward methanol oxidation. *Int J Electrochem Sci.* 2013;8(6):7510–7517.
- [21] Yi L, Liu L, Wang X, Liu X, Yi W, Wang X. Carbon supported Pt-Sn nanoparticles as anode catalyst for direct borohydride-hydrogen peroxide fuel cell: Electrocatalysis and fuel cell performance. *J. Power Sources.* 2011;196(15):9924–9930.
- [22] Radmilovic V, Gasteiger HA, Ross Jr. PN. Structure and chemical composition of a supported Pt-Ru electrocatalyst for methanol oxidation. *J Catal.* 1995;154(1):98-106.
- [23] Beyhan S, Leger JM, Kadırgan F. Pronounced synergetic effect of the nano-sized PtSnNi/C catalyst for methanol oxidation in direct methanol fuel cell *J. Applied Catalysis B: Environ.* 2013;130:305–313.
- [24] Elumalai M and Muthukumaran B, Performance of sodium borohydride in membraneless fuel cells. *International Journal of ChemTech Research.* 2015;7(7):3033–3038.
- [25] Elumalai M, Priya M, Kiruthika S, and Muthukumaran B, Effect of acid and alkaline media on membraneless fuel cell using sodium borohydride as fuel. *AFINIDAD LXXII.* 2015;572:309–313.
- [26] Kalaikathir SPR, Begila David S. Synthesis and characterization of nanostructured carbon-supported Pt electrocatalysts for membraneless methanol fuel cells. *International Journal of Modern Science and Technology.* 2016;1(6):199–212.
- [27] Vijayaramalingam K, Kiruthika S and Muthukumaran B, Promoting Effect of Third Metal (M = Ni, Mo and Rh) on Pd–Ir Binary Alloy Catalysts in Membraneless Sodium Perborate Fuel Cells, *International Journal of Modern Science and Technology.* 2016;3(7):257–263.
- [28] Karunakaran C, Kamalam R. Mechanism and reactivity in perborate oxidation of anilines in acetic acid. *J Chem Soc. Perkin Trans.* 2002;2(12):2011–2018.
- [29] Jayashree RS, Yoon SK, Brushett FR, Lopez-Montesinos FR, Natarajan D, Markoski LJ, Kenis PJA. On the performance of membraneless laminar flow-based fuel cells. *J. Power Sources,* 2010;195(11):3569–3578.
- [30] Choban ER, Markoski LJ, Wieckowski A, Kenis PJA. Micro-fluidic fuel cell based on laminar flow. *J Power Sources.* 2004;128(1):54–60.
- [31] Li H, Sun G, Cao L, Jiang L, Xin Q. Comparison of different promotion effect of PtRu/C and PtSn/C electrocatalysts for ethanol-oxidation. *Electrochim Acta.* 2007;52(24):6622–6629.
- [32] Shukla AK, Ravikumar MK, Roy A, Baraman SR, Sarma DD, Arico AS, Electro-oxidation of methanol in sulfuric-acid electrolyte on platized-carbon electrodes with several functional-group characteristics. *J Electrochem Soc.* 1994;141(6):1517–1522.
- [33] Gyenge EL. Electro-oxidation of borohydride on platinum and gold electrodes: implications for direct borohydride fuel cells. *Electrochem Acta.* 2004;49(6):965–978.
